Role of wide contacts in the ac response of a double-barrier structure

Jun Quan and Yabin Yu*
Department of Applied Physics, Hunan University, Changsha 410082, People's Republic of China

Y. H. Tang†
College of Materials Science and Engineering, Hunan University, Changsha 410082, People's Republic of China
(Received 17 January 2006; revised manuscript received 21 March 2006; published 16 May 2006)

The role of wide contacts is investigated in the ac response of a double-barrier structure. Several physical quantities, such as the distributions of internal potential and charge density, capacitance, and low-frequency ac conductance, are calculated. The results show that when the system is far away from resonance, the charge distribution exists only around the barrier regions as a response to the applied voltage, and hence the contacts have almost no effect on the results. In the resonant case or near resonance, the charge distribution displays large peaks in the contact regions, but almost no charge distribution within the conductor. In the case of small transmission probability, we find a considerable amount of charge distribution both in the contact regions and surrounding the double-barrier conductor. Moreover, we find that qualitatively the presence of contacts does not change the main features of the emittance obtained from a calculation that neglects the widening of contacts. But the contact effect on the capacitance is significant when the chemical potential is very close to the resonant energy: There is a sharp capacitance peak at the resonance, which corresponds to the charge peaks in the contact regions.

DOI: 10.1103/PhysRevB.73.195314 PACS number(s): 73.61.−r, 73.23.Ad

I. INTRODUCTION

The study of electron transport in nanostructure systems is a rapidly developing field of research, and the ac properties of ultrasmall conductors are important for many applications. One of these studied system is a one-dimensional (1D) device connected to wide reservoirs. In these systems, electron-electron (*e*-*e*) interaction is of fundamental importance.[1–11] For the dc case, the effect of *e*-*e* interaction on quantum transport in a quantum wire was studied using the Luttinger liquid model,[12–16] which explains the renormalization of charge density and scattering at impurities.[11,13,16–18] Moreover, the electron interaction is important in the nonlinear transport through mesoscopic systems. For instance, as shown in Refs. 1 and 2, in the presence of a magnetic field the interaction is responsible for the departure of the differential conductance from the Onsager relations. This has been verified experimentally by Zumbuhl *et al.*[3] and Leturcq *et al.*[4] For the ac case, the interaction plays a key role in ensuring charge (current) conservation and gauge invariance under potential shifts.[5–9] On the other hand, in the ac case, the contacts play an important role[16–19] in the conductance due to its significant interaction with conductors. Since the ac response is strongly sensitive to the distribution of potential and charge in the systems, the variation of potential and accumulation of charge in the contact regions would give a considerable contribution to the capacitance and ac conductance of the system. Büttiker *et al.*[6–9] formulated the theory of ac conductance in the regime of linear response and low frequency based on both continuous and discrete internal potential models.[6–9] In our previous work,[20] a quantum wire with two-dimensional (2D) contacts as a whole system was studied based on Büttiker's theory, and the effect of the contacts on ac conductance and charge distribution in the system was investigated. Moreover, the ac response of a double-barrier system was studied in Ref. 21, where the hyperbolic tangent function was employed to describe the boundaries of 2D contacts, and the mode hopping between different transverse channels was neglected in the scattering process of electrons. In this approximation, each electron is in a single channel all the way throughout the scattering process without being scattered into the other channels, and the calculations of scattering wave functions and scattering matrix were much simplified. In this way, however, the contact regions between 1D and 2D portions have to be divided into a series of thin slices to calculate the wave function of the system, and for avoiding onerous calculations the channel coupling was ignored in the scattering between slices. Therefore, some additional oscillation in the wave function may be caused in the contact regions. To avoid this disadvantage, in this paper we will consider the model for the double barrier with reservoirs, as is shown in Fig. 1. Under this model, by using the mode-matching approach[22] we will take into account the hopping of electrons between different channel in the scattering on the interfaces of different regions.

II. MODEL AND FORMULA

The model that we consider in this paper is a 2D-1D-2D system in the *xy* plane, which includes a double-barrier-structure conductor and two reservoirs, as is depicted in Fig. 1. The length of the 1D system is assumed to be $2d$, and the 2D reservoirs are large enough. We use b for one barrier width and $2c$ for the width of the well (between the two barriers; see Fig. 1). In this work we will explore the linear response of the system to a time-dependent external voltage. When the external voltage is applied to the two 2D reservoirs, first we must consider the process that electrons are

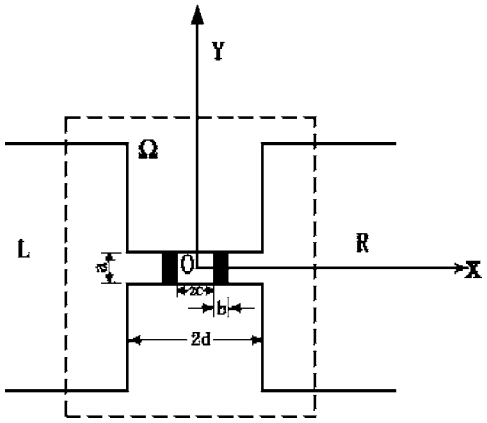

FIG. 1. Schematic view of a double-barrier structure with two reservoirs. Ω is an imagined volume, and is assumed that no electric-field line penetrates the surface of Ω.

injected into the 1D system and then undergo scattering by the contacts and the double barrier, and second we must consider the pile up of charge and the induced internal electrostatic potential affecting the transport of the electrons in the systems. To proceed, we may imagine the volume Ω which includes the whole conductor and parts of the reservoirs (we use the dashed line to indicate it in Fig. 1). It is very large and includes all the varying distributions of the potential and charges. This means that all the electric-field lines come from and end at the charges inside the volume.

In order to calculate the dynamic response of the system with a double barrier, according to Büttiker's theory, we must calculate the injectivity $dn_a(\vec{r})/dE$ and the local density of states (LDOS) $dn(\vec{r})/dE=\Sigma_\alpha dn_a(\vec{r})/dE$ for the system (here $\alpha=L$ for the left contact and $\alpha=R$ for the right contact). As our interest is electron transport in the x direction, we will assume that the potential and charge-density distributions are one dimensional. So we will only calculate the injectivity

$$dn_a(x)/dE = \int [dn_\alpha(\vec{r})/dE]dy \tag{1}$$

and the density of states

$$dn(x)/dE = \int [dn(\vec{r})/dE]dy. \tag{2}$$

In order to do this, we must first calculate the electron wave function of the incoming scattering state (from the left). Consider one electron with wave vector $\vec{K}$ and energy E incident on the channel opening from the left. Its wave function can be written

$$\Psi_l^L(x,y) = \sum_{l'} \left[\delta_{l'l} e^{ik_l^x x} + \left(\frac{v_l}{v_{l'}}\right)^{1/2} s_{11,l'l} e^{-ik_{l'}^x x} \right] \Phi_{l'}^{2D}(y) \quad \text{for } x < -d. \tag{3}$$

For the electron in $x>d$, the wave function reads

$$\Psi_l^R(x,y) = \sum_{l'} \left(\frac{v_l}{v_{l'}}\right)^{1/2} s_{21,l'l} e^{ik_{l'}^x x} \Phi_{l'}^{2D}(y) \quad \text{for } x > d \tag{4}$$

where, for $l' \leqslant \text{int}\left[\left(\frac{2m^* wE}{\pi\hbar^2}\right)^{1/2}\right]$, $s_{11,l'l}$ and $s_{21,l'l}$ are the scattering matrix elements, $v_l=\hbar k_l^x/m^*$ is the incident velocity of the electrons in the direction of transport, and $\Phi_{l'}^{2D}(y)$ are the transverse eigenfunctions of the reservoirs. $k_{l'}^x=[2m^*E/\hbar^2-(l'\pi/w)^2]^{1/2}$ are the vertical components of the incident wave vectors, where w is the width of the 2D portions, m^* is the effective mass of electrons, and E is the energy of the electron. The sum in Eqs. (3) and (4) is taken over all transverse components. l' and $k_{l'}^x$ can be either real or imaginary, i.e., evanescent waves are included.

In the 1D system including the double barrier together with the left and the right leads, it is divided into five portions. The wave function may be expanded as

$$\Psi_l^c(x,y) = \sum_n (A_{nl}^{(I)} e^{ik_n^{(I)x} x} + B_{nl}^{(I)} e^{-ik_n^{(I)x} x}) \Phi_n^{1D}(y) \tag{5}$$

where $I=1,2,3,4,5$ represent the various regions of the double-barrier structure, as shown in Fig. 1. $\Phi_n^{1D}(y)$ are the transverse eigenfunctions of electrons in the 1D system and $k_n^{x(I)}=[2m^*(E-U_I)/\hbar^2-(n\pi/a)^2]^{1/2}$. U_I is the double-barrier potential and given by

$$U_I = \begin{cases} U_0 & \text{in the barriers,} \\ 0 & \text{otherwhere.} \end{cases} \tag{6}$$

On the interface of the barrier, the boundary conditions are that $\Psi(x,y)$ and its derivative $\partial\Psi(x,y)/\partial x$ are continuous. Then we can obtain

$$\sum_n (A_{nl}^{(I)} e^{ik_n^{x(I)} x_I} + B_{nl}^{(I)} e^{-ik_n^{x(I)} x_I}) \Phi_n^{1D}(y) = \sum_n (A_{nl}^{(I+1)} e^{ik_n^{x(I+1)} x_I} + B_{nl}^{(I)} e^{-ik_n^{x(I+1)} x_I}) \Phi_n^{1D}(y) \tag{7}$$

and

$$\sum_n k_n^{x(I)} (A_{nl}^{(I)} e^{ik_n^{x(I)} x_I} - B_{nl}^{(I)} e^{-ik_n^{x(I)} x_I}) \Phi_n^{1D}(y) = \sum_n k_n^{x(I+1)} (A_{nl}^{(I+1)} e^{ik_n^{x(I+1)} x_I} - B_{nl}^{(I)} e^{-ik_n^{x(I+1)} x_I}) \Phi_n^{1D}(y), \tag{8}$$

where x_I is the interface position between regions I and $I+1$. Thus we can obtain the transfer relationship

$$\begin{bmatrix} A^{(I)}(x) \\ B^{(I)}(x) \end{bmatrix} = \prod_{J=I}^{5} M_J \begin{bmatrix} A^{(J)}(x) \\ B^{(J)}(x) \end{bmatrix} \tag{9}$$

where M_J is the transfer matrix element between regions J and $J+1$.

As usual, $\Psi_l^R(x,y)$, $\Psi_l^L(x,y)$, and $\Psi_l^c(x,y)$ need to be matched at $x=-d$ and d. With the requirement that amplitudes and derivatives with respect to x are equal, and after eliminating $s_{11,l'l}$ and $s_{21,l'l}$ from the resulting equations of the matching, we can obtain the following set of linear equations:

$$\sum_n [(T_{mn} - k_n^{x(1)}\delta_{mn})A_{nl}^{(1)} e^{ik_n^{x(1)}d} + (T_{mn} - k_n^{x(1)}\delta_{mn})B_{nl}^{(1)} e^{ik_n^{x(1)}d}] = 2k_l^x M_{lm} e^{-ik_l^x d}, \quad (10)$$

$$\sum_n [(T_{mn} - k_n^{x(5)}\delta_{mn})A_{nl}^{(5)} e^{ik_n^{x(5)}d} + (T_{mn} + k_n^{x(5)}a_{mn})B_{nl}^{(5)} e^{-ik_n^{x(5)}d}] = 0, \quad (11)$$

where $M_{l'n} = \int [\Phi_{l'}^{2D}(y)]^* \Phi_n^{1D}(y) dy$, $k_n^{x(1)} = k_n^{x(3)} = k_n^{x(5)} = [(2m^* E/\hbar^2) - (n\pi/a)^2]^{1/2}$, and $T_{mn} = \Sigma_{l'} k_n^x (M_{l'm})^* M_{l'n}$.

The scattering matrix elements $s_{11,l'l}$ and $s_{21,l'l}$ can be calculated by

$$s_{11,l'l} = -\delta_{l'l}\left(\frac{v_{l'}}{v_l}\right)^{1/2} e^{-i(k_{l'}^x + k_l^x)d} + \sum_n \left(\frac{v_{l'}}{v_l}\right)^{1/2} M_{l'n}(A_{nl}^{(1)} e^{-i(k_n^{(1)x} + k_{l'}^x)d} + B_{nl}^{(1)} e^{i(k_n^{(1)x} - k_{l'}^x)d}),$$

$$s_{21,l'l} = \sum_n \left(\frac{v_{l'}}{v_l}\right)^{1/2} M_{l'n}(A_{nl}^{(5)} e^{i(k_n^{(5)x} - k_{l'}^x)d} + B_{nl}^{(5)} e^{-i(k_n^{(5)x} + k_{l'}^x)d}). \quad (12)$$

Combining Eqs. (3)–(12), we can obtain all the coefficients $A_{nl}^{(l)}, B_{nl}^{(l)}$ and the wave functions of the electrons in the system, and then the injectivity

$$\frac{dn_L(x)}{dE} = \sum_l \int dE\left(-\frac{\partial f}{\partial E}\right) \int dy \frac{1}{hv_l} |\Psi_l(x,y)|^2. \quad (13)$$

For our symmetrical system,

$$\frac{dn_R(x)}{dE} = \frac{dn_L(-x)}{dE} \quad (14)$$

and the LDOS is given by

$$\frac{dn(x)}{dE} = \frac{dn_L(x)}{dE} + \frac{dn_R(x)}{dE}. \quad (15)$$

In the presence of a small and low-frequency ac voltage v_{ac} applied to the reservoir, the internal potential $U(x)$ is given by $U(x) = u_\alpha(x) v_{ac}$, where $u_\alpha(x)$ is the characteristic function. Using the Thomas-Fermi approximation, the characteristic function $u_a(x)$ must satisfy the Poisson equation[6,8]

$$\nabla^2 u_a(\vec{r}) = -\frac{e^2}{\varepsilon_0}\left(\frac{dn_\alpha(\vec{r})}{dE} - \frac{dn(\vec{r})}{dE} u_a(\vec{r})\right), \quad \alpha = 1,2. \quad (16)$$

Under the Thomas-Fermi approximation, the first term on the right of Eq. (16) gives clearly the injected charges and second term gives the induced charges in the conductor. The Thomas-Fermi approximation is based on the assumption that the screened potential is slowly varying in space. In a confined system this assumption is not always satisfied because the potential may not be slowly varying on the interface. However, for atoms this approximation can give a good description of the atomic potential and charge distribution.[23] So, as pointed out in Ref. 24, the assumption does not seem unduly restrictive. On the other hand, in this paper we do not attempt to make a very accurate calculation, and our interest is to present a qualitative estimate for the potential and charge distribution. To give the screened potential for long-range Coulomb interaction, we have employed the Poisson equation. If the sample is close to a gate (see, for instance, Ref. 25), the Coulomb interaction is strongly screened due to the gate and becomes effectively short ranged. We neglected the variation of the potential in the transverse direction and assumed that the characteristic function was a function of x only. This assumption is reasonable, because the variation of potential in fact is induced by the electrochemical potential difference $\delta\mu$ (or external voltage v_{ac}) between the left and right sides. We obtain the following equation by integrating over the transverse direction:

$$-\frac{d^2 u_a(x)}{d^2 x} + \frac{e^2}{\varepsilon_0 A(x)} \frac{dn(x)}{dE} u_a(x) = \frac{e^2}{\varepsilon_0 A(x)} \frac{dn_\alpha(x)}{dE}, \quad \alpha = 1,2, \quad (17)$$

where $A(x) = a \times h$ is the cross-sectional area of the double-barrier structure, and h is the thickness of the system. Since we have a hard-wall potential in the transverse direction, it is reasonable to define the area.

III. RESULTS AND DISCUSSION

A. Internal potential and charge density

First we will calculate the internal potential $u_a(x)$ by numerically solving the Poisson equation (17), and then obtain the induced charge distribution. To solve Eq. (17) for $u_a(x)$, we need the boundary values of $u_a(x)$. Here we use the neutrality condition to determine the boundary values of $u_a(x)$,

$$u_a(x_L) = \frac{dn_a(x_L)}{dE} \Big/ \frac{dn(x_L)}{dE} \quad \text{and} \quad u_a(x_R) = \frac{dn_a(x_R)}{dE} \Big/ \frac{dn(x_R)}{dE} \quad (18)$$

where x_L and x_R are the left and right boundary lines of the region Ω (see Fig. 1), which is a volume[6,8,9] that is so large that electric-field lines vanish through the surface of the volume, i.e., the electric field is almost shielded in the region Ω. We can imagine that the width of the reservoirs is very large; then from Eq. (18) we can conclude that the boundary values $u_1(x_L)$ $[u_2(x_R)]$ and $u_1(x_R)$ $[u_2(x_L)]$ are very close to unity (zero), respectively. When our system is biased by a small voltage δV (it is applied to the 2D reservoir), the distribution of charge density in the region Ω is given by $\delta q = \rho(x)\delta V$, where $\rho(x)$ is defined as

$$\rho(x) = \frac{dq(x)}{dV} = -\varepsilon_0 A(x) \frac{d^2 u_a(x)}{d^2 x} = e^2\left(\frac{dn_a(x)}{dE} - \frac{dn(x)}{dE} u_a(x)\right). \quad (19)$$

In Figs. 2(a)–2(c), we present the distribution of internal potential $u = u(x)$ and charge density $\rho(x)$ for various Fermi levels μ $(= \mu_L = \mu_R)$ at temperature $T = 0$. Here, we use

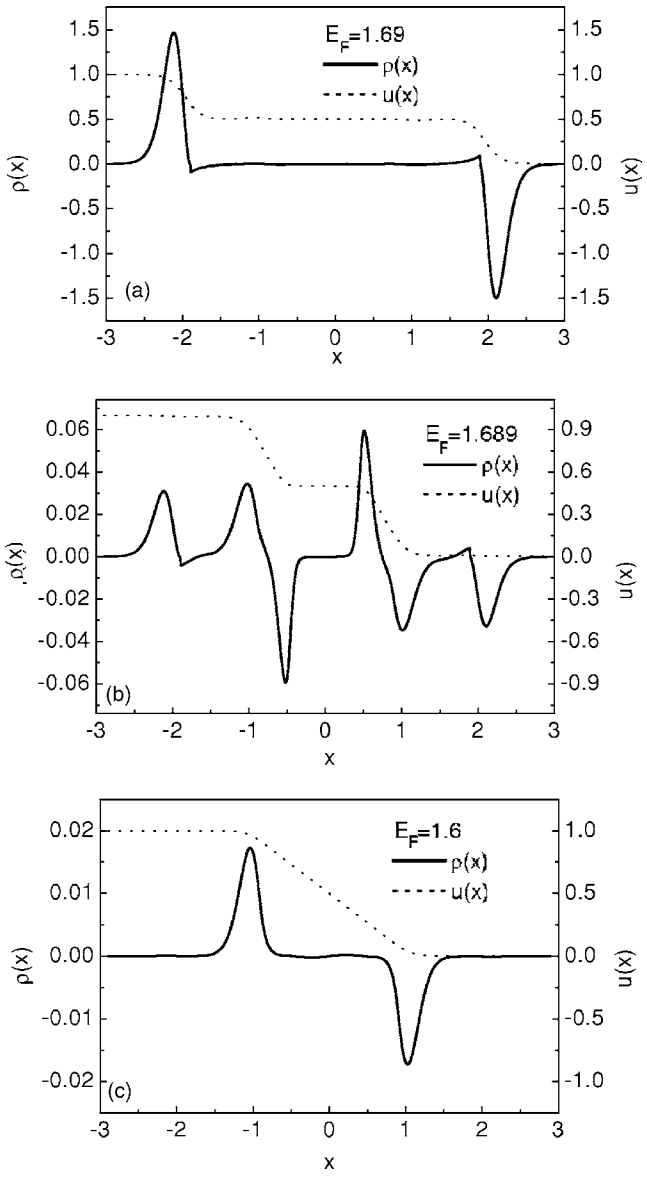

FIG. 2. Distribution of internal potential and density for μ =(a) 1.690, (b) 1.689, and (c) 1.600. Other parameters are a =5 nm, h=0.2, c=0.5, b=0.4, d=1.9. The energy is in units of the transverse ground-state energy $\Delta=h^2/8ma^2$ of the 1D leads, and the width a of the leads is the unit of distance.

$\Delta=h^2/8ma^2$, the energy of the transverse ground state in the 1D leads as a unit of energy, and the width a of the leads as a unit of distance. In our calculation, we set a=5 nm, h =0.2, c=0.5, b=0.4, d=1.9, w=30, and $x_L=-x_R$. The number of channels in the wide contacts, $N_l=3l_{max}$, where l_{max} $=\text{int}\left[\left(\frac{2m^*wE}{\pi\hbar^2}\right)^{1/2}\right]$ is the maximum channel number that make k_l^x take a real value. Similarly, the number of channels in the 1D regions $N_n=\max[3n_{max},3]$, where $n_{max}=\text{int}\left[\left(\frac{2m^*aE}{\pi\hbar^2}\right)^{1/2}\right]$.

Figure 2(a) shows the results for μ=1.690, which corresponds to the resonant case where the Fermi level equals the resonant energy of the double-barrier structure. In this case for an open channel the transmission probability equals unity. In this figure, we find that the potential is constant in the 2D leads but declines when it penetrates the contact. It stays at $u(x)=1/2$ in the 1D part of the system though there is a double-barrier structure, and begins to decrease to zero on the right of it. From the profile of $\rho(x)$, we can find that it only positive and negative peaks occur on the left and right ends of the structure and there is almost no charge accumulation inside the conductor. This reflects the effect of contacts on the distributions of potential and charge density. In the resonant case, the electrons can penetrate completely through the barrier, and the charges driven by the voltage stay neither around nor inside the double-barrier structure. In this case, the scattering of electrons is completely due to the nonuniform cross section in the contact regions, and this scattering results in the potential drops and charge accumulation in the transition regions between the 1D and 2D parts. From our previous work[26] about a 1D double-barrier structure without contacts, the potential drop in the resonant case was almost zero and there is almost no charge accumulation in the system.

In Fig. 2(b), we present the results for low transmission probability, where μ=1.689 and it departs from the resonant energy somewhat. In this case the transmission is small but not zero. In the figure, we find that the potential function $u(x)$ is constant in the lead and gradual declines on the left of the structure to the left barrier. It holds as $u(x)=1/2$ in the 1D part and begins to decrease to zero when it penetrates the right barrier. From the profile of $\rho(x)$, we can see that some positive and negative peaks occur around the barriers, and the charge on the two sides of the barrier has different sign. This corresponds to the junction capacitance produced by the barriers.

Figure 2(c) shows the result for the case where chemical potential (μ=1.600) is far from the resonant energy (μ =1.690) and for all channels the transmission probability is almost zero. The profile of $\rho(x)$ shows that the charge accumulates on the side of the barrier and there are almost no charges in the well. Here the potential function $u(x)$ starts decreasing on the left of the left barrier. The curve of the potential is almost a straight line in the well between the barriers. It stays at $u(x)=1$ and $u(x)=0$ on the left and right of the double-barrier conductor, respectively. It is worth emphasizing that our results for the system with wide contacts show that the characteristic function tends to 1 (0) on the left (right) of the double-barrier conductor for both resonant and nonresonant cases. This satisfies the requirement of Büttiker's theory.[6]

B. Capacitance, dipoles, and low-frequency admittance

We have studied the distributions of internal potential and charge density above. Now we will study the capacitance and ac conductance, which may present a result that is capable of being directly verified by experimental data. According to Eq. (19), when the voltage δV is applied to the left 2D reservoir, the total positive (or negative) charge accumulated in Ω is given by (it should be noticed that the total charge accumulation in the system is zero due to the charge conservation)

$$\delta Q = \frac{1}{2}\int_{x_L}^{x_R} |\delta q(x)| dx, \tag{20}$$

and then, for the symmetric system the capacitance of the structure may be defined as

$$C = \frac{\delta Q}{\delta V} = \int_{x_L}^{0} |\rho(x)| dx = \int_{x_L}^{0} e^2 \left| \frac{dn_a(x)}{dE} - \frac{dn(x)}{dE} u_a(x) \right| dx. \tag{21}$$

We have difficulty in giving a precise definition of the capacitance for our system because our model is a continuous model. In the cases of Figs. 2(a) and 2(c), it seems to be proper that we regard the system as a single capacitor, but in Fig. 2(b) it seems to be better to define the junction capacitance (related to the barriers) and contact capacitance. Here, the definition of the capacitance in Eq. (21) is only to illustrate the behavior of charge accumulation or total capacitance. Since there is no gate, the total charge accumulation in the system is zero. It might be useful to consider the dipole moment p of the structure and the junction dipole moment (corresponding to the left barrier) p_J, and they can be defined as

$$p = \int_{x_L}^{x_R} x\rho(x) dx \tag{22}$$

and

$$p_J = \int_{0}^{b+c+0.4} (x - c - b/2)\rho(x) dx. \tag{23}$$

Using the information about the partial density of states (PDOS), injectivity, and internal potentials, we may calculate the admittance for low frequencies[6,8,9]

$$g_{a\beta}(\omega) = g_{a\beta}(0) - i\omega e^2 E_{\alpha\beta,} \tag{24}$$

where ω is the frequency of the ac bias. $g_{a\beta}(0)$ is the dc conductance, and

$$E_{\alpha\beta} = e^2 \left(\frac{dN_{\alpha\beta}}{dE} - \int dx \frac{dn_a(x)}{dE} u_\beta(x) \right). \tag{25}$$

$E_{\alpha\beta}$ is the emittance. Because of charge conservation, all the emittance elements are equal in magnitude (differing only in sign). In the first term of Eq. (25),

$$\frac{dN_{\alpha\beta}}{dE} = \frac{1}{4\pi i} \int dE \left(-\frac{\partial f}{\partial E} \right) T_r \left(s_{\alpha\beta}^{\div} \frac{ds_{\alpha\beta}}{dE} - \frac{ds_{\alpha\beta}^{+}}{dE} s_{\alpha\beta} \right) \tag{26}$$

are the partial densities of states, and may be interpreted as the carrier density of states in volume Ω, corresponding to those carriers injected from reservoir β and going out of reservoir α. It should be noticed that Eq. (26) is exact only when Ω is infinite ($|x_L| \to \infty$).[27] For the finite-size system, the PDOS is completely expressed by local quantities inside the scattering volume and thus can be computed accurately for any system size,

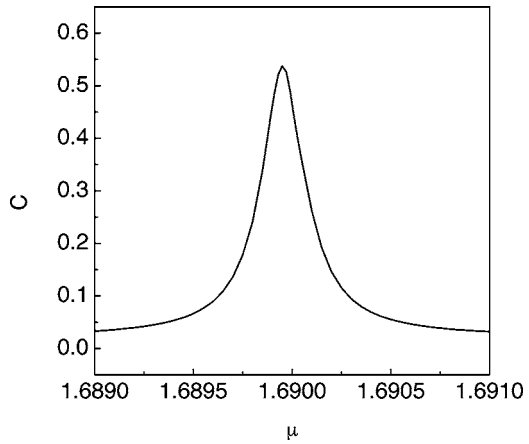

FIG. 3. Capacitance as a function of chemical potential μ, starting from far away from the resonance. The parameters are the same as in Fig. 2.

$$\frac{dN_{\alpha\beta}}{dE} = \frac{-1}{4\pi i} \int dE \left(-\frac{\partial f}{\partial E} \right) T_r \left(s_{\alpha\beta}^{\div} \frac{ds_{\alpha\beta}}{dU} - \frac{ds_{\alpha\beta}^{+}}{dU} s_{\alpha\beta} \right). \tag{27}$$

We make use of a mathematical identity

$$\frac{ds_{\alpha\beta}}{dU} = \int_{x_L}^{x_R} \frac{\delta s_{\alpha\beta}}{\delta U} dx \tag{28}$$

where $ds_{\alpha\beta}/dU$ can be calculated as follows. In the considered region Ω where there is a constant potential U applied, we repeat the above process of calculating the wave functions, and get the scattering matrix element $s_{\alpha\beta}(E,U)$. So we can obtain

$$\frac{ds_{\alpha\beta}}{dU} = \int_{x_L}^{x_R} \frac{\delta s_{\alpha\beta}}{\delta U} dx = \left. \frac{ds_{\alpha\beta}(E,U)}{dU} \right|_{U=0}. \tag{29}$$

In Fig. 3 we present the capacitance $C(\mu)$ as a function of chemical potential around the resonant energy (1.69). From the profile of $C(\mu)$, we find that when the chemical potential approaches the resonant energy, the capacitance increases rapidly and makes a sharp and narrow positive peak at the resonant energy. But when the chemical potential moves away a little from the resonance energy, the capacitance decreases rapidly. It is obvious that this peak originates from the effect of contact. The large capacitance peak corresponds to the peaks of charge in Fig. 2(a).

In Fig. 4(a) we plot the magnitude of the dipole moment $(-p)$ as a function of chemical potential around the resonant energy (μ=1.690). The figure shows that when the chemical potential approaches the resonant energy, the magnitude of the dipole moment increases until it reaches a peak at the resonant energy. The behavior of the dipole moment is similar to that shown for the capacitance in Fig. 3. We present the calculated results for the junction dipole moment in Fig. 4(b). Here, in order to reduce the influence of the charges induced by the contact, we take longer 1D leads (d=2.4).

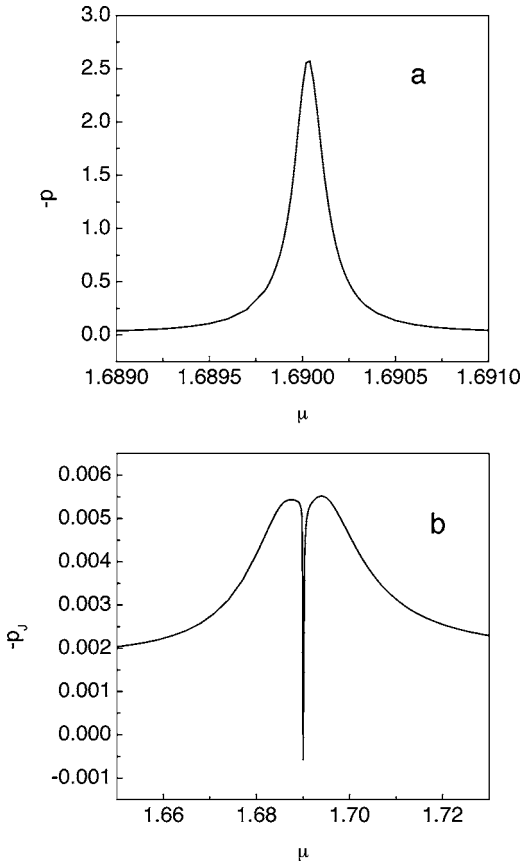

FIG. 4. (a) The dipole moment of the double barrier and (b) the junction dipole moment as functions of chemical potential μ around the resonant energy. Here $d=2.4$, and the other parameters are the same as in Fig. 2.

From the figure, one can find that when the chemical potential approaches the resonant energy ($\mu=1.690$), the junction dipole moment increases first, and then decreases and makes a sharp drop at the resonant energy. This clearly indicates that when the system approaches the resonant state, a considerable amount of electrons start to penetrate through the barriers, and the accumulated charges around the barriers increase with the increase of chemical potential μ. The charges have different sign on the two sides of a barrier. Thus the magnitudes of the junction dipole moments increase with increasing μ at first. However, when μ is very close or equal to the resonant energy the electrons penetrate through the barriers without any scattering, and the accumulated charges around the barriers vanish rapidly. One may notice that the curve drops to negative values (instead of zero) at the resonance. This is ascribed to charges induced by the contact.

Since the emittance elements are equal in magnitude, we only present the emittance element $E_{11}(\mu)$, which is plotted as a function of chemical potential around the resonant energy in Fig. 5. As a comparison, the curve of $C(\mu)$ is plotted in the figure. Here we select another resonant energy of the system ($\mu=3.723$) to describe the ac response of a double-barrier structure. From the profile of them, we can see that the capacitance and the emittance tend to the same values when the chemical potential is away from the resonant energy, but when the system approaches the resonance energy, the difference between them becomes very large. The capacitance increases slowly when the system gradually approaches the resonance energy, but the emittance begins to decrease rapidly when it approaches the resonant energy. We can also see that the capacitance reaches a positive peak when the chemical potential is about 3.723, but the emittance reaches a negative peak. The difference between them is enlarged rapidly near the resonance. By the way, we find the behavior of capacitance in Figs. 3 and 4 is somewhat different. The peak in the latter is widened due to the increase of Fermi energy. This is because the energy levels of the quasibound states in the quantum well between the barriers should have a finite width due to tunneling. With the increase of Fermi energy, the tunneling is enhanced, and the width of the energy levels will be increased.

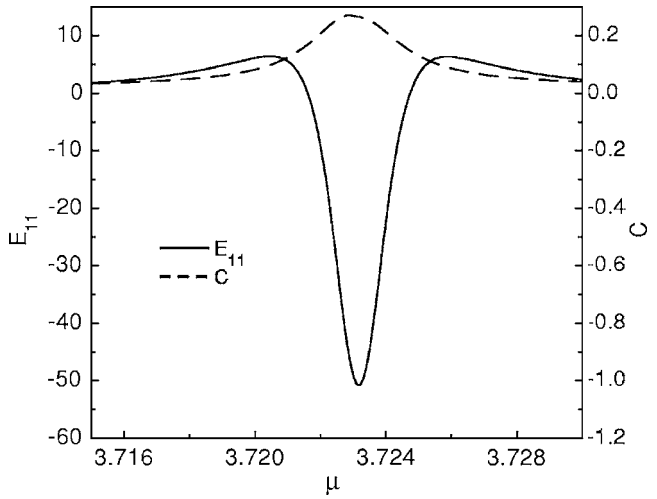

FIG. 5. Capacitance and emittance as functions of chemical potential μ, which start from far away from the resonance. The parameters are the same as in Fig. 2.

IV. CONCLUSION

We have studied the dynamic response of a double-barrier conductor with two contacts, and calculated the distributions of charge density and internal potential, capacitance, dipole moment and low-frequency ac conductance by using the scattering theory developed by Büttiker and co-workers. The results show that when the system is at or close to resonance, where the Fermi energy is close to the resonant energy of the system, the charge distribution displays large peaks in the contact regions, but there is almost no charge distribution in the conductor. While the system is far away from resonance, the charge distribution exists only around the barrier regions as a response to the applied voltage, and hence the contacts have almost no effect on the charge distribution. When the system deviates somewhat from the resonance (the case of small transmission probability), we find a considerable

amount of charge distribution both in the contact regions and surrounding the conductor. Moreover, we find that qualitatively the presence of contacts does not change the main features of the emittance without contacts. But the contact effect on the capacitance is significant when the chemical potential is very close to resonant energy: there is a sharp capacitance peak at resonance that corresponds to the charge peaks in the contact regions.

*Corresponding author: Electronic address: phy_yabinyu@yahoo.com.cn
†Corresponding author: Electronic address: yhtang@hnu.cn

[1] D. Sanchez and M. Büttiker, Phys. Rev. Lett. **93**, 106802 (2004).
[2] B. Spivak and A. Zyuzin, Phys. Rev. Lett. **93**, 226801 (2004).
[3] D. M. Zumbuhl, C. M. Marcus, M. P. Hanson, and A. C. Gossard, cond-mat/0508766 (unpublished).
[4] R. Leturcq, D. Sanchez, G. Gotz, T. Ihn, K. Ensslin, D. C. Driscoll, and A. C. Gossard, Phys. Rev. Lett. **96**, 126801 (2006).
[5] R. Landauer, Phys. Scr., T **42**, 110 (1992).
[6] M. Büttiker, J. Phys.: Condens. Matter **5**, 9361 (1993).
[7] A. Prêtre, H. Thomas, and M. Büttiker, Phys. Rev. B **54**, 8130 (1996).
[8] M. Büttiker, H. Thomas, and A. Prêtre, Z. Phys. B: Condens. Matter **94**, 133 (1994).
[9] M. Büttiker, A. Prêtre, and H. Thomas, Phys. Rev. Lett. **70**, 4114 (1993).
[10] H. J. Schulz, G. Cuniberti, and P. Pieri, cond-mat/9807366 (unpublished).
[11] J. Voit, Rep. Prog. Phys. **58**, 977 (1995).
[12] M. Ogata and H. Fukuyama, Phys. Rev. Lett. **73**, 468 (1994).
[13] F. D. M. Haldane, J. Phys. C **14**, 2585 (1981).
[14] C. L. Kane and M. P. A. Fisher, Phys. Rev. B **46**, 15233 (1992).
[15] Siddhartha Lal, Sumathi Rao, and Diptiman Sen, Phys. Rev. Lett. **87**, 026801 (2001).
[16] D. L. Maslov and M. Stone, Phys. Rev. B **52**, R5539 (1995).
[17] I. Safi and H. J. Schulz, Phys. Rev. B **52**, R17040 (1995).
[18] V. V. Ponomarenko, Phys. Rev. B **52**, R8666 (1995).
[19] A. Yu. Alekseev and V. V. Cheianov, Phys. Rev. B **57**, R6834 (1998).
[20] Y. B. Yu, T. C. Au Yeung, and W. Z. Shangguan, Phys. Rev. B **66**, 235315 (2002).
[21] T. C. Au Yeung, Y. B. Yu, and W. Z. Shangguan, Phys. Rev. B **68**, 075316 (2003).
[22] G. Kirczenow, Phys. Rev. B **39**, R10452 (1989).
[23] L. D. Landau and E. Lifshitz, *Quantum Mechanics: Non Relativistic Theory* (Addison-Wesley, Reading, MA, 1958).
[24] G. D. Mahan, *Many-Particle Physics* (Plenum Press, New York, 1981).
[25] V. V. Ponomarenko, Phys. Rev. B **54**, 10 328 (1996); Y. M. Blanter, F. W. J. Hekking, and M. Büttiker, Phys. Rev. Lett. **81**, 1925 (1998).
[26] W. Z. Shangguan, T. C. Au Yeung, Y. B. Yu, C. H. Kam, and X. Zhao, Phys. Rev. B **65**, 235315 (2002).
[27] Q. Zheng, J. Wang, and H. Guo, Phys. Rev. B **56**, 12462 (1997).